Accepted Manuscript

DFT and spectroelectrochemical study of cyanate adsorption on gold single crystal electrodes in neutral medium

W. Cheuquepán, J.M. Orts, A. Rodes, J.M. Feliu

PII: S1572-6657(16)30531-8
DOI: doi:10.1016/j.jelechem.2016.10.011
Reference: JEAC 2878

To appear in: *Journal of Electroanalytical Chemistry*

Received date: 29 July 2016
Revised date: 5 October 2016
Accepted date: 7 October 2016

Please cite this article as: W. Cheuquepán, J.M. Orts, A. Rodes, J.M. Feliu, DFT and spectroelectrochemical study of cyanate adsorption on gold single crystal electrodes in neutral medium, *Journal of Electroanalytical Chemistry* (2016), doi:10.1016/j.jelechem.2016.10.011

DFT and spectroelectrochemical study of cyanate adsorption on gold single crystal electrodes in neutral medium.

W. Cheuquepán, J.M. Orts* [†#], A. Rodes* [†], J.M. Feliu* [†]*

[†]Departamento de Química Física e *Instituto Universitario de Electroquímica, Universidad de Alicante, Apartado 99, E-03080 Alicante, SPAIN.

Corresponding autor : jm.orts@ua.es

Keywords:
cyanate adsorption, DFT, IRRAS, cyclic voltammetry, Au(111), Au(100), gold single crystal electrodes

ABSTRACT

The adsorption of cyanate anions at Au(111) and Au(100) single crystal electrodes has been studied spectroelectrochemically in neutral solutions. Potential-dependent in situ InfraRed Reflection Absorption spectra obtained below the onset of cyanate oxidation were compared with previously published data and analyzed on the basis of periodical Density Functional Theory (DFT) calculations. The calculated adsorption energies for cyanate and related species suggest that cyanic and isocyanic acid adsorb weakly at the studied gold surfaces and, thus, seems not to be at the origin of any of the adsorbate bands in the experimental infrared spectra collected in the cyanate-containing solutions. The latter features can be clearly ascribed to the asymmetric OCN stretching of N-bonded cyanate species. The observation of absorption bands in a wide spectral region, including features above 2200 cm^{-1}, agrees with the coexistence of N-bonded cyanate species with different adsorption sites and tilting angles. DFT calculations have revealed that although these adspecies can have significantly different frequencies, their adsorption energies are rather close. In addition, the existence of collective in-phase vibrations at relatively high cyanate coverages also contributes to the widening of the absorption bands.

1. INTRODUCTION

The adsorption and oxidation of cyanate anions have been studied at various electrode materials such as gold [1-4] , platinum [1,5-7], silver [8,9] and copper [2,10]. In some papers, the formation of adsorbed cyanate has been reported as a product of the electrochemical oxidation of several related substances such as cyanide [6,11], thiocyanate [12], glycine [13,14] or semicarbazide [15]. On the other hand, the presence of adsorbed cyanate species has been spectroscopically detected as a product of some reactions between CO and NO at various solid/gas interphases [16-19].

From in situ external reflection infrared spectra, several authors have detected the formation of carbon dioxide as the main product of cyanate electrooxidation, this process being paralleled by the consumption of dissolved cyanate anions [1,4-6]. Kitamura et al [6] proposed a bimolecular decomposition involving two adsorbed cyanate species, yielding carbon dioxide and nitrogen. The adsorption of cyanate was detected as a potential-dependent competitive process as witnessed by the observation of a band around 2220 cm^{-1} for adsorbed cyanate. This feature was ascribed by most authors to N-bonded cyanate anions [1,4-6,8,9]. Bron and Holze [2] proposed that adsorbed cyanate could occupy bridge adsorption sites at low coverages. Yépez and Scharifker [5] found from their in situ infrared spectra that cyanate can chemisorb dissociatively on platinum electrodes yielding carbon monoxide which would be formed from adsorbed cyanate with a flat orientation. They also concluded that adsorbed cyanate can rearrange from flat to terminal orientation as witnessed by infrared absorption bands detected around 2200-2300 cm^{-1} for all the surfaces studied. Besides, Corrigan and Weaver [1] and Kitamura et al. [6] observed both for platinum [1,6] and gold [1] electrodes a band at ca. 2260 cm^{-1} that was attributed to the isocyanic acid resulting from the protonation of cyanate anions induced by the protons released upon the electrochemical oxidation of the electrode surface.

The experimental findings described above can be compared with the results derived from theoretical studies published in the literature for cyanate and related species both adsorbed or in gas, solution or solid phases. In this way, results for non-adsorbed species can be taken as a reference for the analysis of the stability of the corresponding adsorbed phases. In this respect, the results for cyanic and isocyanic species are relevant for the identification of some experimental spectroscopic features that have been assigned to these species in previous papers. Schuurman et al [20] found from their calculated standard enthalpies in gas phase, that the isocyanic acid isomer (HNCO) is more stable than cyanic acid (HOCN) by about a significant 102 $kJ \cdot mol^{-1}$ (-115.37 $kJ \cdot mol^{-1}$ versus -12.96 $kJ \cdot mol^{-1}$).

Some theoretical studies of the vibrational spectrum of isocyanic acid in the gas phase have been reported by the groups of Durig [21], Lowenthal [22] and Teles[23]. Zabardasti et al. [24] studied the microsolvation of isocyanic acid with water (1 to 4 molecules) using perturbation theory (MP2) and Density Functional Theory (DFT). They reported the formation of strong hydrogen bonds between water and cyanate, with cooperative effects appearing when increasing the number of water molecules, that do not modify significantly the vibrational frequencies corresponding to the asymmetric (at ca. 2340 cm^{-1}, changes smaller than 30 cm^{-1}) and symmetric (around 1340 cm^{-1}, changes smaller than 10 cm^{-1}) OCN stretching modes of the isocyanic acid.

The theoretical study of the adsorption of cyanate species on metals, has focused mainly on the (100) surface of some fcc metals. Yang and Whitten [25,26] found that the stability order for cyanate on Ni(100) cluster model surfaces was 4-fold > bridge > atop, in all cases with the molecular axis perpendicular to the metal surface. The maximum variations in adsorption energy with surface site amounted to around 54 $kJ{\cdot}mol^{-1}$. Regarding the bonding mode, N-bonded (isocyanate) was more stable than O-bonded (cyanate) by around 63 $kJ{\cdot}mol^{-1}$ (in average). Their calculated adsorption energies for the 4-fold sites were -430 and -364 $kJ{\cdot}mol^{-1}$, respectively. These authors also considered the possibility of a side-on adsorption of cyanate, or a significant tilting from the surface normal. Increasing the tilt angle from the normal leads to a decrease in the absolute value of the adsorption energy. Regarding the adsorption parallel to the surface, the most stable geometry had an adsorption energy of -351 $kJ{\cdot}mol^{-1}$, significantly smaller than for the N-bonded normal adsorption, but similar to the O-bonded cyanate with its axis perpendicular to the metal surface.

Different groups have also studied the adsorption of cyanate on Cu(100) cluster surfaces [27-29]. Some discrepancy exists regarding the most stable adsorption site. Garda et al [28] obtained that the 4-fold hollow site was the most favourable, while Hu et al[29] observed that the bridge site was slightly more favourable for cyanate adsorption. From the results of Garda et al [27] it can be concluded that the size and type of cluster strongly affects the calculated adsorption energy values.

Belelli et al [28] have studied the chemisorption of N-bonded cyanate on Pd(100) at different coverages. Another study regarding the interaction of OCN with metals is that of Ferullo and Castellani [29] who carried out a DFT analysis of the transition states involved in the formation of OCN on a Rh dimer from adsorbed CO and NH species. We are not aware of any previous work reporting a theoretical study of the adsorption of cyanate species on gold surfaces.

All the previous spectroelectrochemical studies dealing with adsorbed cyanate on metals have been carried out in potential regions where significant oxidation of cyanate or other species takes place. It can be also remarked that the significant width of absorption bands attributed in previous works to adsorbed cyanate terminally coordinated to the surface suggests that they probably originate from the contributions of different adsorption sites. Moreover, the nature of the adsorbed species formed in the cyanate-containing solutions (either N- or O-bonded cyanate or the corresponding protonated forms) is a point still open to discussion. In this work we have focused our study on the Au(100) and Au(111) surfaces, in the so-called double-layer potential regions, where the adsorbed species formed from solution cyanate can adsorb while avoiding significant anodic faradaic currents. We have also avoided high cyanate concentrations, as the cyanate ligand can facilitate the oxidation and dissolution of the surface metal atoms by forming soluble complexes of Au(I). Our objectives are to verify the presence of adsorbed cyanate or related species, and to elucidate the origin of the observed splittings/shifts in frequency. In order to support the interpretation of the experimental spectra, in particular the band assignments, we have carried out a theoretical study using periodic DFT calculations. We have studied the effect of surface crystallographic orientation, surface site (bonding mode) and molecular orientation on the adsorption energy, geometry and harmonic vibrational frequencies of the candidate species to be adsorbed under our experimental conditions.

In order to decide on the eventual formation of protonated forms of adsorbed cyanate (such as cyanic (HOCN) or isocyanic (HNCO) acids) we have extended our DFT calculations to these species. We have not taken into consideration the adsorption of other isomers such as HONC or HCNO (fulminic acid), and their anions, as these species are highly unstable. The calculated standard enthalpies of formation reported by Schuurman et al [20] amount to around +235 and +171 $kJ \cdot mol^{-1}$, respectively, for these acids.

2. EXPERIMENTAL

Working solutions were obtained by dissolving the corresponding amount of the sodium cyanate (96% Sigma Aldrich) and sodium perchlorate (99.99%, Sigma Aldrich) in ultrapure water (18.2 MΩ·cm, Elga Vivendi). These solutions were deaerated with Ar (N50, Air Liquide) and blanketed with the same gas during the experiments.

Clavilier's method [30,31] was employed to prepare, from a 99,9998% gold wire (Alfa-Aesar), the Au(111) and Au(100) single crystals used as working electrodes in the electrochemical (ca. 2.0 mm

in diameter) and in situ external reflection infrared spectroscopy experiments (diameter around 4.5 mm). Prior to each experiment, these electrodes were heated in a gas-oxygen flame, cooled down in air and protected with a droplet of ultrapure water [31-33].

All the voltammetric and in situ infrared experiments were performed in glass cells using a gold wire and a Ag/AgCl/Cl^-(sat) electrode (connected to the corresponding cell through a Luggin capillary) as the counter and the reference electrodes, respectively. The spectroelectrochemical cells used in this work are equipped with a prismatic CaF_2window beveled at 60° [34,35]. In situ infrared experiments were carried out using a Veemax (Pike Tech.) reflectance accessory placed in the main chamber of a Nexus 8700 (Thermo Scientific) spectrometer equipped with a MCT-A detector. All the spectra were collected with a resolution of 8 cm^{-1} and are presented in absorbance units (a.u.) as $-\log(R/R_o)$, where R and R_o represent the single beam sample and reference reflectivity spectra, respectively. Thus, positive-going and negative-going bands correspond, respectively, to the gain and loss of species for the sample spectrum with respect to the reference spectrum. Sets of 200 interferograms were collected at different sample potentials and referred to a reference single beam spectrum collected in the cyanate-containing solutions at -0.50 V.

3. COMPUTATIONAL DETAILS

All the periodic DFT calculations were carried out using the Vienna Ab-Initio Simulation Program (VASP, version 4.6) code [36-39], using the Projector-Augmented-Wave method [40,41], with the GGA functional of Perdew, Burke and Ernzehof [42,43] and a cutoff energy of 400 eV.

The periodic models for the unreconstructed, non-relaxed, Au(111) and Au(100) surfaces consisted of (3x3) simulation cells formed by 4 metallic layers (9 atoms each), for a total of 36 metal atoms. The slabs were separated by a vacuum region of more than 1.2 nm, that ensures that no significant coupling exists between periodic replica in the Z-direction. The metal nuclei coordinates were kept fixed, with a lattice constant of 0.41748 nm (nearest-neighbor distances of 0.29520 nm). This value, obtained from a series of bulk energy calculations with different lattice constants, and fitting to the Murnaghan equation of state, coincides with the values reported by other authors using the PBE functional, and compares well with the experimental value of 0.4065 nm for pure gold [44].

Calculations of systems including metallic slabs used the automatic Monkhorst-Pack [45] (7x7x1) scheme, for sampling the Brillouin zone. Methfessel-Paxton [46] smearing was used with

sigma=0.2 eV. As convergence criteria we used: 10^{-6} eV for the electronic energy, and forces on atoms below 0.02 eV/Angstrom, for the geometry optimization (without restrictions) of the molecular adspecies. The calculated vibrational frequencies were obtained using the harmonic approximation, with atomic displacements of 0.02 Angstrom. For most calculations, and unless otherwise stated, the (3x3) simulation cell contained only one adsorbate species on one side of the slab, this situation corresponding to the low coverage limit (θ = 1/9), where lateral interactions between adsorbates are expected to be minimal or almost negligible.

In the case of gas-phase molecular systems, the simulation cell was a cubic box (20 Angstrom side length) containing a single molecular species. Integration in the Brillouin zone only used the gamma point. Smearing choice was Gaussian (with sigma=0.1 eV). As convergence criteria for the free molecular species we chose 10^{-6} eV for the electronic energy, and forces on atoms below 0.002 eV/Angstrom, for the geometry optimization. For the gas phase OCN radical, all the results reported correspond to spin-polarised calculations. All other calculations have been carried out without spin polarisation.

Unless otherwise stated, all the energy values reported correspond to electronic energy, without including ZPE correction, as we have verified that the vibrational energy contribution is very small (about 1% of the adsorption energy values without correction). The visualization of the molecular optimized geometries and vibrational modes has been done using Molden [47] and Jmol [48].

4. EXPERIMENTAL RESULTS AND DISCUSSION.

4.1. Voltammetric experiments.

Figure 1A shows cyclic voltammograms obtained with a Au(100) electrode in contact with a 0.08 M sodium perchlorate solution with a cyanate concentration equal to 1 mM. After immersion of the flame annealed electrode at - 0.50 V, the electrode potential was cycled from -0.55 to +0.66 V, thus excluding the potential range where the electrode surface and/or cyanate anions are oxidized. In comparison with the voltammetric response recorded in the cyanate-free solution (curves a), a significant charge contribution associated to the presence of cyanate is detected for potentials above -0.20 V. A well-marked oxidation peak at 0.25 V in the first positive-going scan can be related to the lifting of the surface reconstruction typical for the flame-annealed electrode surface [32,33], which appears at ca. 0.50 V in the bare sodium perchlorate solution. The negative shift of this voltammetric feature is typical and indicative of the presence of specifically adsorbed species [32].

In the second and subsequent voltammetric cycles, the aforementioned peak is shifted to slightly less positive potentials as compared to the first voltammetric cycle, its charge density decreasing to a stationary value. The latter is related to the fraction of the electrode surface which is again reconstructed during the voltammetric excursion into the lower potential region [32,33].

The voltammetric behavior observed in experiments carried out in cyanate-containing solutions with concentrations ranging from 0.01 to 50 mM is essentially similar to that described above for the 1 mM solution. Curves shown in Figure 1C correspond to the first voltammetric cycle recorded in the same potential window as in Figure 1A for solutions with various cyanate concentrations. The observed voltammetric features show higher charge densities for increasing cyanate concentrations. Note that the peak for the lifting of the surface reconstruction is shifted to less positive potentials under these conditions, becoming sharper for cyanate concentrations up to 1 mM but broadening again for concentrations above this latter concentration value. The cyclic voltammograms recorded in the 10 and 50 mM cyanate solutions show the existence of an irreversible oxidation process for potentials above 0.40 V.

Similar voltammetric curves are shown in Figures 1B and D for the Au(111) electrode. Two differences can be remarked when comparing these curves with those reported above for Au(100). The first one regards the height of the peak related to the lift of the characteristic reconstruction of the Au(111) surface [32,33], which is much less defined than for Au(100). Secondly, irreversible oxidation currents appear for the Au(111) electrode for cyanate concentrations above 1 mM, giving rise to a well-defined voltammetric peak at ca. 0.50 V for this latter concentration value. This peak disappears for higher cyanate concentrations leading to voltammetric profiles which are more similar to those observed for the Au(100) electrode.

The voltammetric charges associated to the presence of cyanate were measured in order to have a rough estimation of the coverage of adsorbed species attained for Au(100) and Au(111) electrodes in the cyanate-containing solutions. Thus, voltammetric currents were integrated for the stationary curves recorded for each cyanate concentration in the potential window shown in Figure 1. The charge density value obtained for the cyanate-free sodium perchlorate solution (uncorrected for the corresponding double layer contribution) was subtracted from the latter values in order to estimate the contribution coming from cyanate adsorption. The resulting values range from 8 to 57 $\mu C \cdot cm^{-2}$ in the case of Au(100) when increasing the cyanate concentration from 0.01 to 50 mM. Values for the Au(111) electrode under the same conditions range from 3 to 72 $\mu C \cdot cm^{-2}$. Compared to the charge density corresponding to a monolayer (1 adsorbate species for each gold surface atom of the

(1x1) surfaces) on the basis of one electron exchanged per adsorbed species (i.e 184 and 212 $\mu C \cdot cm^{-2}$ for Au(100) and Au(111), respectively) the maximum coverage value attained (at ca. +0.66 V) would be for both electrode surfaces in the range around 0.3 OCN species per Au surface atom.

4.2. In situ infrared spectroscopy experiments.

Figure 2 show sets of potential-dependent infrared spectra collected with either p- or s-polarized light for Au(111) and Au(100) electrodes in a 50 mM NaNCO + 0.08 M $NaClO_4$ solution. Such a relatively high cyanate concentration (above 10 mM) facilitates the achievement of a good enough signal to noise ratio in the external reflection configuration. The spectra are referred to a single beam spectrum collected at -0.50 V in the same solution. Well-defined negative-going bands appear at 2167 cm^{-1} for potentials above -0.40 V for the Au(111) electrode and above -0.2 V for Au(100) in the experiments carried out with p-polarised light. This band is also present in the spectra collected with s-polarised light. The intensity of the band at 2167 cm^{-1} increases both for Au(111) and Au(100) as the electrode potential is increased up to 0.66 V. Taking into account the surface selection rule for external reflection infrared spectroscopy experiments on metals [49], that precludes the observation of adsorbed species when using a s-polarized beam, it can be concluded that the former band corresponds to non-adsorbed species. Several authors [1,2,5,6] have assigned the feature at 2167 cm^{-1} to the asymmetric OCN stretching of dissolved cyanate anions, which are depleted from the solution thin layer (formed between the electrode and the infrared window) as a consequence of their adsorption and/or oxidation at the electrode surface (vide infra).

Other features observed in the spectra collected in the cyanate-containing solutions are positive-going bands at 2343 and 2170-2250 cm^{-1}. The former band can be related to the asymmetric OCO stretching of dissolved carbon dioxide molecules which are formed upon cyanate oxidation [1,2,5,6] and accumulate in the thin solution layer. This irreversible process takes place at potentials above 0.40-0.50 V and can be related to the observation of irreversible oxidation currents in this potential range (see figure 1).

The positive-going bands above 2170 cm^{-1} partially overlap with the cyanate consumption band, specially for the less positive electrode potentials. Since these bands are not observed in the spectra collected with s-polarised light it can be stated that, according to the surface selection rule, they correspond to a vibration mode for an adsorbed species which gives rise to non-zero change of the dynamic dipole of the molecule in the direction normal to the electrode surface. Two contributions can be appreciated in the potential-dependent spectra obtained for the Au(100) electrode. As it can

be observed in Figure 2 and in the plots of the potential-dependent band frequencies (Figure 3), a contribution appearing at ca. 2200 cm^{-1} is the main feature of the spectra collected up to 0.20 V. For more positive potentials, the main feature is observed at ca. 2250 cm^{-1} with the contribution at lower wavenumbers appearing as a shoulder. In the case of the Au(111) electrode, some positive-going contribution seems to appear also below 2167 cm^{-1} for potentials up to 0.40 V. The overlapping of this feature with the negative-going band for dissolved cyanate makes difficult to assign an accurate band frequency value.

Note that the development of the positive-going features above 2170 cm^{-1} is paralleled by that of the negative going band at 2167 cm^{-1} in the case of the Au(100) electrode. However, in the case of the Au(111) electrode this latter feature is detected for potentials above -0.40 V, whereas the positive-going features are clearly observed for potentials more positive than 0.30 V. The overlapping between negative- and positive-going bands in the same spectral region makes difficult the quantitative analysis of these features. In this way, the absence of a clear positive-going feature does not mean necessarily that there is not some absorption from adsorbed species at the sample potential, the latter being cancelled in the spectra by its overlapping with the negative-going feature for the depleted cyanate anions in solution. However, it is also possible that some adsorbed species could exist without giving any infrared absorption, due to flat lying orientation, whereas the consumption of solution species could be detected. Finally, the depletion of solution cyanate can also be related to irreversible cyanate oxidation. However, the latter process takes place at potentials above 0.40 V as witnessed by the observation of the band for carbon dioxide. From all these observations, it can be concluded that the appearance of the band for depleted cyanate anions can be roughly taken as an indication of the occurrence of adsorption/desorption processes, irrespectively of the nature and orientation of the adsorbed species. Note, that the onset of the observation of the band at 2167 cm^{-1} in Figure 2 is well below the potential of zero charge for the corresponding gold electrode surface [50,51] thus suggesting the strong specific adsorption of species coming from dissolved cyanate.

5. COMPUTATIONAL RESULTS AND DISCUSSION.

5.1. Cyanate radical, cyanic acid and isocyanic acid in gas phase.

Table 1 summarizes the geometric data and harmonic vibrational frequencies obtained in our DFT calculations for the neutral cyanate radical, cyanic acid and isocyanic acid in the gas phase. These

results are provided in order to compare with the respective data for the different adsorbates considered. Bond distances and angles agree reasonably well with those reported from calculations using different levels of theory [20,21]. In particular, the loss of linearity of the OCN backbone in the structures of both acids is well reproduced. From our results, of the two isomers, isocyanic acid (HNCO) is more stable than cyanic acid (HOCN) by about 1,3 eV (125 kJ/mol) at 0K. This energy difference is slightly higher than that found by Schuurman et al [20] (103 kJ/mol) using a highly accurate level of theory.

5.2. Adsorption of cyanate on Au(111) and Au(100) surfaces. N-bonded vs O-bonded vs flat.

In order to know about the relative stability of the different bonding modes of cyanate (parallel to the surface, N-bonded, O-bonded), on the different surface sites of Au(111) and Au(100), we have studied the adsorption on top, bridge, and hollow sites of these surfaces. Once established the optimized geometries of the adsorbates, we have also calculated their vibrational frequencies within the harmonic approximation. Optimized geometries of the N-down cyanate adsorbate with different bonding configurations are shown in figures 4 and 5, for Au(100) and Au(111), respectively. Calculated adsorption energies and vibrational frequencies are summarized in tables 2 and 3 for Au(100) and Au(111) respectively. The adsorption energies have been referred to the cyanate radical in gas phase and the clean Au(hkl) model slab surface. The zero-point vibrational energy correction has not been included, as we have verified that it amounts to only about 1% of the non-corrected adsorption energy value.

A first conclusion that can be drawn from these data is that both O-down and N-down bonding (both with the OCN axis normal to the surface and tilted) strongly stabilize adsorbed OCN species versus the gas phase, but the N-down form is significantly more stable, by more than 100 $kJ \cdot mol^{-1}$. This indicates that N-bonding is expected to prevail on the Au(100) and Au(111) surfaces. Regarding the relative stabilities of the adsorption sites on Au(100), in the case of N-down the most favourable geometry corresponds to the bridge site, followed by the 4-fold site (about 22 $kJ \cdot mol^{-1}$ less stable), and finally the top position (less stable than the bridge by around 29 $kJ \cdot mol^{-1}$). The adsorption energies referred to the gas phase range from -213 to -184 $kJ \cdot mol^{-1}$. In the case of O-down adsorption, the adsorbate stability decreases in the order: 4-fold >= bridge > top, with the adsorption energy (referred to the gas radical OCN) going from -96 $kJ \cdot mol^{-1}$ for the hollow site to -73 $kJ \cdot mol^{-1}$ for the top coordination. In all the previous cases, the molecular axis is oriented essentially normal to the metal surface. As the energy difference between adsorption sites is comparable to the average thermal energy (RT at 298 K amounts to ca. 25 $kJ \cdot mol^{-1}$) coexistence of

more than one bonding type is to be expected at room temperatures.

Regarding the calculated infrared frequencies, we will focus on the asymmetric OCN stretching, which is the vibration detected under our experimental conditions. Note that, the obtained external reflection spectra do not show any detectable band around 1300 cm^{-1} that could be ascribed to the symmetric mode. The only experimental bands attributable to adsorbed cyanate are observed between 2100 and 2250 cm^{-1} and correspond to the asymmetric OCN stretch. It must be remarked that the type of adsorption site influences the value of these frequencies in a significant amount. These shifts can amount to near 90-100 cm^{-1} in the case of the asymmetric OCN stretching, upon changing of the adsorption site.

In the previous cases (N-down and O-down), the optimized geometry for the three adsorption sites has the molecular axis perpendicular to the surface. We also carried out optimizations starting from several geometries with the cyanate molecular axis oriented quasi-parallel to the metal surfaces. We found two local minima characterized by adsorption energies very close to those of the bridge perpendicular adsorption. In both of them, the bonding to the metal involves the N atom. In the first one (Figure 4E), the N atom is located on the bridge site, but the molecular axis is significantly tilted from the normal (by about 45º), with the oxygen atom located approximately above the center of the (1x1) primitive cell, i.e., above the 4-fold site. In the second one (Figure 4D), the N atom is slightly displaced from the vertical of the top site, and the molecular axis is tilted by 62º from the normal, and is aligned with the diagonal of the (1x1) primitive cell. The adsorption energies are very close to those for the non-tilted cyanate adsorption on the same sites. This means that significant tiltings of the molecular axis from the surface normal do not suffer from strong energy penalties. We can expect that the adsorbed cyanate can present a distribution of axis tilt values. This tilt can be affected, of course, by interactions either between neighbouring cyanate adsorbates (that can become important at intermediate and high coverages), and with interfacial water molecules (including hydrogen bonding). The vibrational frequencies of the tilted adsorbates are slightly redshifted with respect to those of the normal N-bonded but still in the range observed experimentally.

The adsorption energies obtained by us for N-down cyanate are considerably lower than those reported from DFT calculations of cyanate adsorbed on Pd(100) (around -280 kJ/mol [28]), Ni(100) surface (-430 $kJ \cdot mol^{-1}$ [25]) or Cu(100) (-330 $kJ \cdot mol^{-1}$, [27,52]) surfaces. This is in agreement with the more noble character of the gold metal, as compared with Cu, Ni, Pd, which in general are much more reactive. It must also be kept in mind that the theoretical calculations of these other groups

used cluster models, which are known to provide a much poorer description of the metals than the periodic models used here. In particular, this is evidenced by the very strong dependence of the adsorption energies found by Garda et al for different copper clusters [27].

In the case of Au(111), we found that both the N-bonded and the O-bonded forms have adsorption energies smaller than those on Au(100). The adsorption energy of the N-form ranges from -170 to -190 kJ·mol^{-1} on Au(111), with rather small differences for different adsorption sites. If we compare these values against the values on Au(100), - 180 to -213 kJ·mol^{-1}, we can conclude that adsorption of cyanate on Au(111) is not very site-sensitive. In the case of the O-form we find values from -50 to -70 kJ·mol^{-1} on Au(111) while they amount to -72 to -96 kJ·mol^{-1} on Au(100). On the basis of these values we can conclude that O-bonded cyanate adsorption is not expected to take place.

The effect of the adsorption site on the frequency of the OCN stretch is smaller than on the Au(100) surface, with a maximum difference of about 60 cm^{-1} for the N-down adsorbate. However, the differences between the frequencies of N-down and O-down are greater than for Au(100). On Au(111) they range from 150 to 200 cm^{-1}.

A number of geometry optimizations were carried out starting from several configurations having the molecular axis of cyanate either parallel or close to parallel to the Au(111) surface. These structures evolved towards reducing the tilt of the molecular axis with respect to the normal. Two optimized geometries were found, both N-down. One with the N atom located on-top of a Au atom (Figure 5D), and the other one very close to the bridge position (Figure 5E). The adsorption energies are almost identical to those of the non-tilted adsorbates on the same sites. This means that, as in the case of Au(100), a distribution of orientations of the molecular axis of adsorbed cyanate is expected.

5.3. Adsorption of cyanic acid (HOCN) and isocyanic (HNCO) acid on Au(111) and Au(100) surfaces.

We have also studied the adsorption of acidic forms as some authors [1,6] have invoked their formation from in situ infrared experiments. The most favourable configuration (with adsorption energy of -40 kJ·mol^{-1} referred to the gas phase) of cyanic acid on Au(100) corresponds to bonding to the top site, with the nitrogen atom slightly shifted in the direction of the diagonal of the surface unit cell (Figure 6A). The molecular plane is perpendicular to the metal surface, and it is aligned

with the diagonal of the primitive (1x1) unit cell of the metal surface. The hydrogen atom is pointing towards the metal surface and is located approximately above the hollow site. The most important difference with respect to the geometries obtained with adsorbed cyanate is the very strong tilting (around 76º) of the OCN axis with respect to the surface normal. This means that the molecular axis is nearly parallel to the metal surface, and that the dynamic dipole corresponding the the OCN stretchings would have a very small component in the z direction. This, according to the surface selection rule for adsorbates on metals, would make its detection very difficult, if not impossible, in the spectroelectrochemical experiments. Another adsorption geometry with slightly smaller adsorption energy is the tilted bridge (Figure 6B). In this configuration, obtained after optimization starting from the hollow site, the hydrogen and nitrogen atoms are both above bridge sites, and the molecular plane is perpendicular to the surface, and parallel to the surface atomic dense rows. The molecular axis is even more tilted (by more than 80º) with respect to the normal. A third local minimum was found corresponding to bonding to the bridge site, but only with the nitrogen atom. The OCN axis is aligned with the metal surface dense rows, and the OH bond is rotated by about 45º from this direction. In this case the tilt from the normal was much smaller (about 20º), but the weaker adsorption energy and long N-Au distance (greater than 300 pm) would correspond to a physisorbed species.

Conversely, cyanic acid is very weakly adsorbed on Au(111) surfaces. The most stable adsorption site is on top of a surface gold atom (-6,5 $kJ \cdot mol^{-1}$), while the bridge, tetrahedral hollow and octahedral hollow have energies between -3,7 and -3,9 $kJ \cdot mol^{-1}$. The molecular orientation is with the OCN axis essentially perpendicular to the metal surface (Figures 6C and D). There is no modification of the geometric parameters and vibrational frequencies with respect to those reported in Table 1 for gas phase cyanic acid. This, together with N-metal distance values, indicates a very weak, physical in origin, interaction with the metal surface.

Regarding the adsorption of isocyanic acid (HNCO), we found that for both Au(111) and Au(100) surfaces, and independently of the type of adsorption site, we obtain geometries with the OCN axis perpendicular to the metal surface, and with very low adsorption energies. Moreover, no significant difference was observed with respect to the internal geometry and vibrational frequencies of the free molecule. This indicates that there is no clear preference for the adsorption on a particular type of surface site and points to a physisorption behaviour, which is confirmed by the separation of the O atom from the surface metal atoms (around 380 pm), and by the adsorption energies (referred to the acid in gas phase in all cases) between -6.7 and -7.0 $kJ \cdot mol^{-1}$ for the Au(100) surface, and around -2.0 $kJ \cdot mol^{-1}$ for Au(111) (all significantly lower than the average thermal energy, which

amounts to about 25 kJ·mol^{-1} at 300K). This means that we can essentially rule out the possibility of having adsorbed isocyanic acid on these gold electrode surfaces in our experimental conditions. This contrasting behavior between the cyanic and isocyanic acids is attributable to the strong difference in energy in the gas phase, with the isocyanic acid been much more stable, together with the differences in energy depending on the bonding atom (N-bonding to the metal being much more favorable than O-bonding, as it follows from the data with the cyanate adsorbate).

Taking into account that the most stable (thermodynamically favoured) acid isomer (isocyanic acid) does not present significant adsorption energies on the two gold surfaces studied, and that cyanic acid only chemisorbs relatively weakly on Au(100), and with molecular orientations significantly tilted from the surface normal (almost parallel to the metal surface), we can conclude that the protonated forms of cyanate are not expected to be relevant for interpreting the spectroelectrochemical results. It must be kept in mind that solvation interactions would stabilize the acids with respect to the gas phase, and that the presence of other adsorbed species (either solvent or solutes) would make the adsorption of the cyanic and isocyanic acids even more difficult.

5.4. Effect of coverage on the vibrational frequencies of adsorbed cyanate.

In order to have some feeling about the effect of coverage on the adsorption energetics and on the vibrational frequencies of the cyanate adsorbates, we carried out some calculations having more than one adsorbate on the (3x3) model slab used in all the calculations reported in this paper. We restricted our tests to the Au(100) surface. We have not carried out a complete study of the dependence of adsorption geometry, energy and frequencies on coverage, as it is out of the scope of the paper. We have limited our study of the coverage effect to two situations. The full monolayer with a cyanate species adsorbed per surface metal atom, and coverages comparable to that estimated from the integration of the voltammetric current densities. In all the calculations the adsorbed cyanate was oriented in the most favourable way, N-down.

For the full monolayer, (θ =1) with 9 cyanate species adsorbed on the surface of the Au(100)-(3x3) slab, three different starting configurations were considered:

a) with all the 9 N-down cyanate species adsorbed on top sites.
b) with all the 9 N-down cyanate species occupying bridge sites.
c) a mixed layer with the N-down cyanate occupying 6 bridge sites (in two rows) and 3 top sites (in

a row).

The latter adlayer was selected as this configuration was expected. from the previous calculations, to be energetically more favourable in order to minimize repulsive interactions between neighbouring adspecies. This was later confirmed by a value of energy significantly more negative than for the single-site full occupancy configuration (even of the most stable site at low density). However, it must be taken into account that, because of the (3x3) periodicity of the simulation cell used, that would not necessarily be the most favorable adlayer arrangement. It can be expected that an adlayer formed by alternating rows that are composed by all-top and all-bridge N-down cyanate would probably yield lower energy. It must be taken into account also that we have carried out no dipole-correction. Moreover, formation of hydrogen bonds with the interfacial solvent molecules can influence the ordering in the adlayer, as the difference in energy between the bridge and top sites of N-down cyanate is relatively small.

The calculation of the vibrational frequencies after optimization of the high-density adlayers put into evidence additional details to account for when interpreting the experimental spectra. Among the calculated values of frequency for the asymmetric OCN stretching, some of them were significantly higher (in the range between 2208 and 2280 cm^{-1}), while some other were in the range between 2169 and 2188 cm^{-1}. The higher values correspond to the cooperative, all-in-phase vibrations of the asymmetric OCN stretching collective mode, while the lower frequencies correspond to the modes having molecules with some dephasing in their vibrational motion with respect to the others. This coupling-induced vibrational frequency shift has been previously put in evidence in DFT calculations of adsorbed species (see works by the groups of Sautet [53,54] and Ricart [55]) and would contribute to the broadening of the absorption bands.

We also studied theoretically the optimized geometry and harmonic vibrational frequencies of three different adlayers on the Au(100)-(3x3) slab, having cyanate coverages closer to the maximal coverage estimated from the voltammetric integrated charge density involved in cyanate adsorption:
a) two adlayers with 3 cyanates per surface unit cell, all with bridge bonding ($\theta = 1/3$). These two adlayers differ in the initial positions chosen to bond the N atom, that is, in the relative distances between the cyanate adsorbates.
b) one adlayer with 4 cyanates adsorbed on bridge positions ($\theta = 4/9$)

The behavior observed for the calculated frequencies for these three later adlayers essentially reproduced the splitting of the frequencies into lower and higher frequency ranges, which varied

depending on the particular structure. The full frequency range for the calculated asymmetric stretching went from 2167 cm^{-1} to 2284 cm^{-1}, values that practically coincide with those observed for the full coverage (θ= 1) cyanate adlayers.

This means that this frequency splitting will also contribute to the observation of infrared absorption by N-bonded cyanate in a rather wide frequency range, irrespectively of the bonding mode of the adsorbed cyanate.

6. CONCLUSIONS.

The experimental spectroelectrochemical results reported in this work prove the formation of strongly adsorbed species on Au(100) and Au(100) in contact with neutral cyanate-containing solutions. The potential-dependent adsorption/desorption processes take place in the so-called double-layer region, at potentials significantly lower than the threshold for cyanate electrooxidation. The presence of adsorbed species is reflected by the typical negative shift of the voltammetric peak for the lift of the corresponding surface reconstruction. Moreover, in situ IRRAS spectra show bands related to the adsorption/desorption processes, including bands for adsorbed species and for the depletion of dissolved cyanate. These bands appear in the spectra at potentials well bellow the potential of zero charge for the Au(111) and Au(100) electrode surfaces. Adsorbate bands appear in a wide frequency range between ca. 2170 and 2250 cm^{-1} as previously reported by different authors that ascribed them either to adsorbed cyanate or to its protonated form, isocyanic acid.

From detailed DFT calculations of optimized geometries and theoretical frequencies for the different candidate adspecies and surface adsorption sites, the following conclusions can be drawn:

Regarding cyanate adsorption:

- Optimized geometries obtained from DFT calculations indicate that, both on the Au(100) and on the Au(111) surfaces cyanate bonding to the surface is especially favoured when it involves coordination of the nitrogen atom to the surface gold atoms (as compared to bonding by the oxygen atom).

- On Au(100), when cyanate adsorbs perpendicular to the metal, the bridge site is more stable than the others by 20-30 $kJ{\cdot}mol^{-1}$. On Au(111) the differences are even smaller, below 14 $kJ{\cdot}mol^{-1}$. These

are not big energy differences as compared to the thermal energy RT, which means that coexistence of N-bonded cyanate adsorbed on different surface sites is to be expected.

- Cyanate can also adsorb with significant tilt of the molecular axis with respect to the surface normal (with similar adsorption energies). In the case of this tilt would significantly approach the limiting value of 90º, the z component of the transition dipole corresponding to the OCN stretch (both asymmetric and symmetric) would be small, and difficult, if not impossible to detect at all due to the surface selection rule in external reflection experiments. The overlapping of bands due to solution and adsorbed species in the external reflection experiments complicates the analysis of the effect of the tilting of the OCN axis of adsorbed cyanate on the intensity of the corresponding absorption bands. It must be taken into account that usually, with p-polarised light, the intensity of the positive-going adsorbate bands from vibrational modes with a non negligible component of the dynamic dipole normal to the metal surface is significantly stronger than the negative counterpart corresponding to consumption of randomly oriented solution species. However, for the spectra in Figure 2 collected at the less positive sample potentials, the opposite is observed. Namely, neat negative bands due to the consumption of solution cyanate can be seen in a wide potential range where no distinctive adsorbate bands are detected. This observation suggests that at low coverage the parallel or strongly tilted adsorption geometries are favored (possibly due to interactions with adsorbed water).

- Calculated harmonic vibrational frequencies for the adsorbed cyanate in the different configurations show a significant dependence on the nature of the surface site and coverage.

- Test calculations with adlayers having different coverages of N-bonded cyanate have shown that some splitting of the vibrational frequency value of the asymmetric OCN stretch occurs as a consequence of the collective in-phase vibration at high and intermediate coverages. Besides, from a preliminar subset of results, it can be advanced that the in the most stable ordered adlayer top and bridge adspecies are expected to coexist, as this makes possible an adlayer arrangement that minimizes lateral repulsions between neighbouring adsorbates.

- The latter conclusions allow us to better understand the very wide absorption region where the signal for the asymmetric OCN stretch is observed. The experimental band profile, is in reality a convolution of a number of different signals which slightly differ as a consequence of different bonding and adsorption site, as well as different interactions (including H bonding with interfacial water). A more detailed study would require the deconvolution of the experimental signals for

adsorbed species, which is complicated by the overlapping with solution features, and is out of the scope of this paper.

Regarding cyanic and isocyanic acids:

- The least favourable coordination of the acidic form to the surface corresponds to bonding through the oxygen atom. In the isocyanic acid (HNCO), the N atom, which gives the most favourable coordination to the surface for adsorbed cyanate, is forming a covalent bond with hydrogen. DFT calculations clearly indicate that isocyanic acid is very weakly adsorbed on Au(hkl), the adsorption being inespecific to the surface adsorption site, with its molecular axis slightly tilted (less than 10º) from the normal. The closest atom to the metal surface is in all cases far beyond the usual chemical bonding distances. All these evidences point to a typical physisorption behaviour.

- In the case of cyanic acid (HOCN), the adsorption interaction is slightly stronger (weak chemisorption) than for isocyanic acid on Au(100). Bonding to the surface proceeds through the terminal N atom, and the most estable optimized geometries have the molecular axis nearly parallel to the metal surface (strongly tilted from the surface normal). This would make very difficult the detection of this adspecies, as a consequence of the surface selection rule. In any case, the adsorption energy of the cyanic acid (referred to the gas phase molecule) is not very high. On Au(111), isocyanic acid has adsorption energies as low as those of cyanic acid, indicating that both species are not candidates for competing for the surface adsorption sites with solvent molecules and anions such as cyanate. From these data, the adsorption of either the cyanic or the isocyanic acids is not very likely to take place on the gold surfaces studied in our experimental conditions.

As a general comment, it must be recalled that we have not included in this paper the study of the effect of hydrogen bonding with interfacial water, as this has no significant effect on the frequency of the asymmetric OCN stretch, which is responsible for the main adsorbate band observed. However, because of the formation of strong hydrogen bonds, as concluded from DFT studies of cyanate solvation [24], this could have a significant effect on adlayer energetics and ordering, without discarding the alteration of the relative populations of adsorbed cyanate on the surface.

7. ACKNOWLEDGEMENTS.

The authors acknowledge the funding by Ministerio de Economía y Competitividad (project CTQ2013-44083-P) and the University of Alicante. William Cheuquepán is grateful for the award of a F.P.I. grant associated to project CTQ2009-13142.

FIGURE CAPTIONS.

Figure 1. Cyclic voltammograms obtained for A,C) Au(100) and B,D) Au(111) electrodes in cyanate-containing 0.08 M $NaClO_4$ solutions. Panels A and B show the voltammetric curves obtained during the first (b1) and second (b2) voltammetric cycles between - 0.55 and 0.60 V in a 1mM cyanate solution. Panels C and D allow the comparison of the first voltammetric cycles obtained in x mM NaOCN + 0.08 M $NaClO_4$ solutions (b) 0.01; (c) 0.1; (d) 1: (e) 10 and (f) 50. Curves (a) in all panels correspond to the cyanate-free solution. Immersion potential in all the experiments was -0.50 V. Sweep rate: 50 $mV \cdot s^{-1}$.

Figure 2. Potential-dependent infrared external reflection spectra collected with p- or s-polarized light for Au(111) and Au(100) electrodes in a 50 mM NaOCN + 0.08 M $NaClO_4$ solution. The reference spectrum was collected at -0.50 V in the same solution. 200 interferograms were coadded to obtain each single beam spectrum.

Figure 3. Plot of the potential-dependent band frequencies of absorption bands observed in the in situ infrared spectra collected with Au(100) and Au(111) electrodes in a 50 mM NaOCN + 0.08 M $NaClO_4$ solution. (▼) CO_2, (■) dissolved cyanate, (▲) adsorbed cyanate. Plots for the band frequencies of solution species are given just to indicate the onset of their formation.

Figure 4. Optimized geometries of N-bonded cyanate on Au(100) surface. A) Top ; B) Bridge ; C) Hollow ; D) Tilted-top ; E) Tilted Bridge

Figure 5. Optimized geometries of N-bonded cyanate on Au(111) surface. A) Top ; B) Bridge ; C) Octahedral hollow ; D) Tilted-top ; E) Tilted bridge , F) Tetrahedral hollow

Figure 6. Optimized geometries of adsorbed cyanic acid (HOCN) on Au(100) surfaces (Tilted-top (A) and Tilted bridge (B)) and Au(111) (Bridge (C) and Top (D))

TABLES

Table 1. Optimized geometry and vibrational frequencies of cyanate radical, cyanic acid and isocyanic acid in the gas phase.

Table 2. Calculated adsorption energies, vibrational frequencies and optimized geometry of N-down, O-down and flat OCN adsorbed on Au(100).

Table 3. Calculated adsorption energies, vibrational frequencies and optimized geometry of N-down, O-down and flat OCN adsorbed on Au(111).

Table 4. Calculated adsorption energies, vibrational frequencies and optimized geometry of cyanic acid (HOCN) adsorbed on Au(111) and Au(100).

Reference List

1. D. S. Corrigan and M. J. Weaver, "*Adsorption and oxidation of benzoic acid, benzoate, and cyanate at gold and platinum electrodes as probed by potential-difference infrared spectroscopy*", Langmuir, 4 (1988) 599-606.
2. M. Bron and R. Holze, "*Cyanate and thiocyanate adsorption at copper and gold electrodes as probed by in situ infrared and surface-enhanced Raman spectroscopy*", J. Electroanal. Chem., 385 (1995) 105-113.
3. O. Hofmann, K. Doblhofer, and H. Gerischer, "*Infrared reflection-absorption measurements on emersed gold electrodes*", J. Electroanal. Chem. Interfacial Electrochem., 161 (1984) 337-344.
4. D. S. Corrigan and M. J. Weaver, "*The interpretation of solution electrolyte vibrational bands in potential-difference infrared spectroscopy*", J. Electroanal. Chem., 239 (1988) 55-66.
5. O. Yepez and B. R. Scharifker, "*Mechanistic pathways during oxidation of cyanate on platinum single crystal faces*", Electrochim. Acta, 50 (2005) 1423-1429.
6. F. Kitamura, M. Takahashi, and M. Ito, "*Anodic oxidation of cyanide and cyanate ions on a platinum electrode*", Chem. Phys. Lett., 136 (1987) 62-66.
7. M. Bron and R. Holze, "*Polarization-sensitive in situ infrared spectroscopy. The adsorption of simple ions at platinum electrodes*", Fresenius' J. Anal. Chem., 361 (1998) 694-696.
8. D. S. Corrigan and M. J. Weaver, "*Coverage-dependent orientation of adsorbates as probed by potential-difference infrared spectroscopy: azide, cyanate, and thiocyanate at silver electrodes*", J. Phys. Chem., 90 (1986) 5300-5306.
9. J. D. Roth and M. J. Weaver, "*Potential-difference surfac infrared spectroscopy under forced hydrodynamic flow conditions : control and elimination of adsorbate solution-phase interferences*", Anal. Chem., 63 (1991) 1603-1606.
10. K. Brandt, E. Vogler, M. Parthenopoulos, and K. Wandelt, "*In situ and ex situ FTIR characterization of a cyanate adlayer on Cu(111)*", J. Electroanal. Chem., 570 (2004) 47-53.
11. F. Huerta, C. Mele, B. Bozzini, and E. Morallon, "*Voltammetric and in situ FTIRS study on CN- and Au(CN)x- complexes at the polycrystalline gold surface in citrate medium*", J. Electroanal. Chem., 569 (2004) 53-60.
12. M. Bron and R. Holze, "*The adsorption of thiocyanate ions at gold electrodes from an alkaline electrolyte solution: a combined in situ infrared and Raman spectroscopic study*", Electrochim. Acta, 45 (1999) 1121-1126.
13. L. C. Chen, T. Uchida, H. C. Chang, and M. Osawa, "*Adsorption and oxidation of glycine on Au electrode: An in situ surface-enhanced infrared study*", Electrochem. Commun., 34 (2013) 56-59.
14. C. H. Zhen, S. G. Sun, C. J. Fan, S. P. Chen, B. W. Mao, and Y. J. Fan, "*In situ FTIRS and EQCM studies of glycine adsorption and oxidation on Au(111) electrode in alkaline solutions*", Electrochim. Acta, 49 (2004) 1249-1255.
15. V. Climent, A. Rodes, J. M. Orts, J. M. Feliu, and A. Aldaz, "*The electrochemistry of nitrogen-containing compounds at platinum sing le crystal electrodes: Part 2. Semicarbazide on Pt(100) electrodes*", J. Electroanal. Chem., 436 (1997) 245-255.
16. K. L. Kostov, P. JAKOB, H. RAUSCHER, and D. MENZEL, "*Interaction of CO with O, N and NO on Ru(001) : evidence for bridge-adsorbed CO, site changes and formation of isocyanate species*", J. Phys. Chem., 95 (1991) 7785-7791.
17. O. S. Alexeev, S. Krishnamoorthy, C. Jensen, M. S. Ziebarth, G. Yaluris, T. G. Roberie, and M. D. Amiridis, "*In situ FTIR characterization of the adsorption of CO and its reaction with NO on Pd-based FCC low NOx combustion promoters*", Catal. Today, 127 (2007) 189-198.
18. T. Bansagi, T. S. Zakar, and F. Solymosi, "*An FTIR study on the formation of NCO surface complexes over Rh/CeO2*", Appl. Catal. , B, 66 (2006) 147-150.
19. F. Solymosi, T. Bansagi, and T. Sueli Zakar, "*Surface interaction and reaction of NO + CO on a supported Au catalyst*", Phys. Chem. Chem. Phys., 5 (2003) 4724-4730.
20. M. S. Schuurman, S. R. Muir, W. D. Allen, and H. F. Schaefer, III, "*Toward subchemical*

accuracy in computational thermochemistry: focal point analysis of the heat of formation of NCO and [H,N,C,O] isomers", J Chem Phys, 120 (2004) 11586-11599.
21. J. R. Durig, X. Zhou, N. E. Durig, D. Nguyen, and D. T. Durig, "*Vibrational spectra and structural parameters of some XNCO and XOCN (X=H, F, Cl, Br) molecules*", J. Mol. Struct., 917 (2009) 37-51.
22. M. S. Lowenthal, R. K. Khanna, and M. H. Moore, "*Infrared spectrum of solid isocyanic acid (HNCO): vibrational assignments and integrated band intensities*", Spectrochim. Acta, Part A, 58A (2001) 73-78.
23. J. H. Teles, G. Maier, B. A. Hess, Jr., L. J. Schaad, M. Winnewisser, and B. P. Winnewisser, "*The CHNO isomers*", Chem. Ber., 122 (1989) 753-766.
24. A. Zabardasti and M. Solimannejad, "*Theoretical study and AIM analysis of hydrogen bonded clusters of water and isocyanic acid*", J. Mol. Struct. : THEOCHEM, 819 (2007) 52-59.
25. H. Yang and J. L. Whitten, "*Chemisorption of OCN on Ni(100) - an ab initio study*", Surf. Sci., 401 (1998) 312-321.
26. H. Yang and J. L. Whitten, "*Reaction and adsorption energetics of CN+Oâ†'OCN on nickel*", J. Mol. Struct. : THEOCHEM, 458 (1999) 131-142.
27. G. R. Garda, R. M. Ferullo, and N. J. Castellani, "*Chemisorption of NCO on Cu(100). A density functional theory study*", Surf. Sci., 598 (2005) 57-67.
28. P. G. Belelli, M. M. Branda, G. R. Garda, R. M. Ferullo, and N. J. Castellani, "*Chemisorption of isocyanate (NCO) on the Pd(100) surface at different coverages*", Surf. Sci., 604 (2010) 442-450.
29. R. M. Ferullo and N. J. Castellani, "*NCO formation from CO and NH species over Rh2 A density functional theory study*", J. Mol. Catal. A: Chem., 212 (2004) 359-364.
30. J. Clavilier, D. Armand, S.-G. Sun, and M. Petit, "*Electrochemical adsorption behaviour of platinum stepped surfaces in sulphuric acid solutions*", J. Electroanal. Chem., 205 (1986) 267-277.
31. A. Rodes, E. Herrero, J. M. Feliu, and A. Aldaz, "*Structure sensitivity of irreversibly adsorbed tin on gold single-crys tal electrodes in acid media*", J. Chem. Soc. Faraday. Trans., 92 (1996) 3769-3776.
32. D. M. Kolb, "*Reconstruction phenomena at metal-electrolyte interfaces*", Prog. Surf. Sci., 51 (1996) 109-173.
33. A. Hamelin, "*Cyclic voltammetry at gold single-crystal surfaces .1. Behaviour at low index faces*", J. Electroanal. Chem., 407 (1996) 1-11.
34. A. Rodes, J. M. Pérez, and A. Aldaz, *"Vibrational Spectroscopy"*, in Handbook of Fuel Cells. Fundamentals, Technology and Applications., Vielstich, W., Gasteiger, H. A., and Lamm, A. (Eds.)John Wiley & Sons Ltd., Chichester, 2003, 191-219.
35. J. M. Delgado, J. M. Orts, and A. Rodes, "*ATR-SEIRAS Study of the Adsorption of Acetate Anions at Chemically Deposited Silver Thin Film Electrodes*", Langmuir, 21 (2005) 8809-8816.
36. G. Kresse and J. Hafner, "*Ab initio molecular dynamics of liquid metals*", Phys. Rev. B: Condens. Matter, 47 (1993) 558-561.
37. G. Kresse and J. Hafner, "*Ab initio molecular-dynamics simulation of the liquid-metal-amorphous-semiconductor transition in germanium*", Phys. Rev. B: Condens. Matter, 49 (1994) 14251-14269.
38. G. Kresse and J. Furthmueller, "*Efficient iterative schemes for ab initio total-energy calculations using a plane-wave basis set*", Phys. Rev. B: Condens. Matter, 54 (1996) 11169-11186.
39. G. Kresse and J. Furthmuller, "*Efficiency of ab-initio total energy calculations for metals and semiconductors using a plane-wave basis set*", Comput. Mater. Sci., 6 (1996) 15-50.
40. P. E. Bloechl, "*Projector augmented-wave method*", Phys. Rev. B: Condens. Matter, 50 (1994) 17953-17979.
41. G. Kresse and D. Joubert, "*From ultrasoft pseudopotentials to the projector augmented-wave method*", Phys. Rev. B: Condens. Matter Mater. Phys., 59 (1999) 1758-1775.
42. J. P. Perdew, K. Burke, and M. Ernzerhof, "*Generalized gradient approximation made simple*", Phys. Rev. Lett., 77 (1996) 3865-3868.
43. J. P. Perdew, K. Burke, and M. Ernzerhof, "*Generalized gradient approximation made simple.*

[Erratum to document cited in CA126:51093]", Phys. Rev. Lett., 78 (1997) 1396.
44. W. P. Davey, "*Precision measurements of the lattice constants of twelve common metals*", Phys. Rev., 25 (1925) 753-761.
45. H. J. Monkhorst and J. D. Pack, "*Special points for Brillouin-zone integrations*", Physical Review B-Condensed Matter, 13 (1976) 5188-5192.
46. M. Methfessel and A. T. Paxton, "*High-precision sampling for Brillouin-zone integration in metals*", Phys. Rev. B: Condens. Matter, 40 (1989) 3616-3621.
47. G. Schaftenaar and J. H. Noordik, "*Molden: a pre- and post-processing program for molecular and electronic structures*", J. Comput. -Aided Mol. Des., 14 (2000) 123-134.
48. "*Jmol: an open-source Java viewer for chemical structures in 3D.*", http://www. jmol. org, (2015).
49. R. G. Greenler, "*Infrared study of adsorbed molecules on metal surfaces by reflection techniques*", J. Chem. Phys., 44 (1966) 310-315.
50. J. Lecoeur, J. Andro, and R. Parsons, "*The behavior of water at stepped surfaces of single crystal gold electrodes*", Surf. Sci., 114 (1982) 320-330.
51. A. Hamelin, T. Vitanov, E. S. Sevastyanov, and A. Popov, "*The electrochemical double layer on sp metal single crystals. The current status of data*", J. Electroanal. Chem., 145 (1983) 225-264.
52. J. M. Hu, Y. Li, J. Q. Li, Y. F. Zhang, W. Lin, and G. X. Jia, "*Chemisorption of OCN on Cu (100) surface. A density functional study*", J. Solid State Chem., 177 (2004) 2763-2771.
53. D. Loffreda, D. Simon, and P. Sautet, "*Dependence of stretching frequency on surface coverage and adsorbate-adsorbate interactions: a density-functional theory approach of CO on Pd (111)*", Surf. Sci., 425 (1999) 68-80.
54. D. Loffreda, D. Simon, and P. Sautet, "*Vibrational frequency and chemisorption site: a DFT-periodic study of NO on Pd(111) and Rh(111) surfaces*", Chem. Phys. Lett., 291 (1998) 15-23.
55. D. Curulla, A. Clotet, and J. M. Ricart, "*Adsorption of carbon monoxide on Pt{100} surfaces: dependence of the CO stretching vibrational frequency on surface coverage*", Surf. Sci., 460 (2000) 101-111.

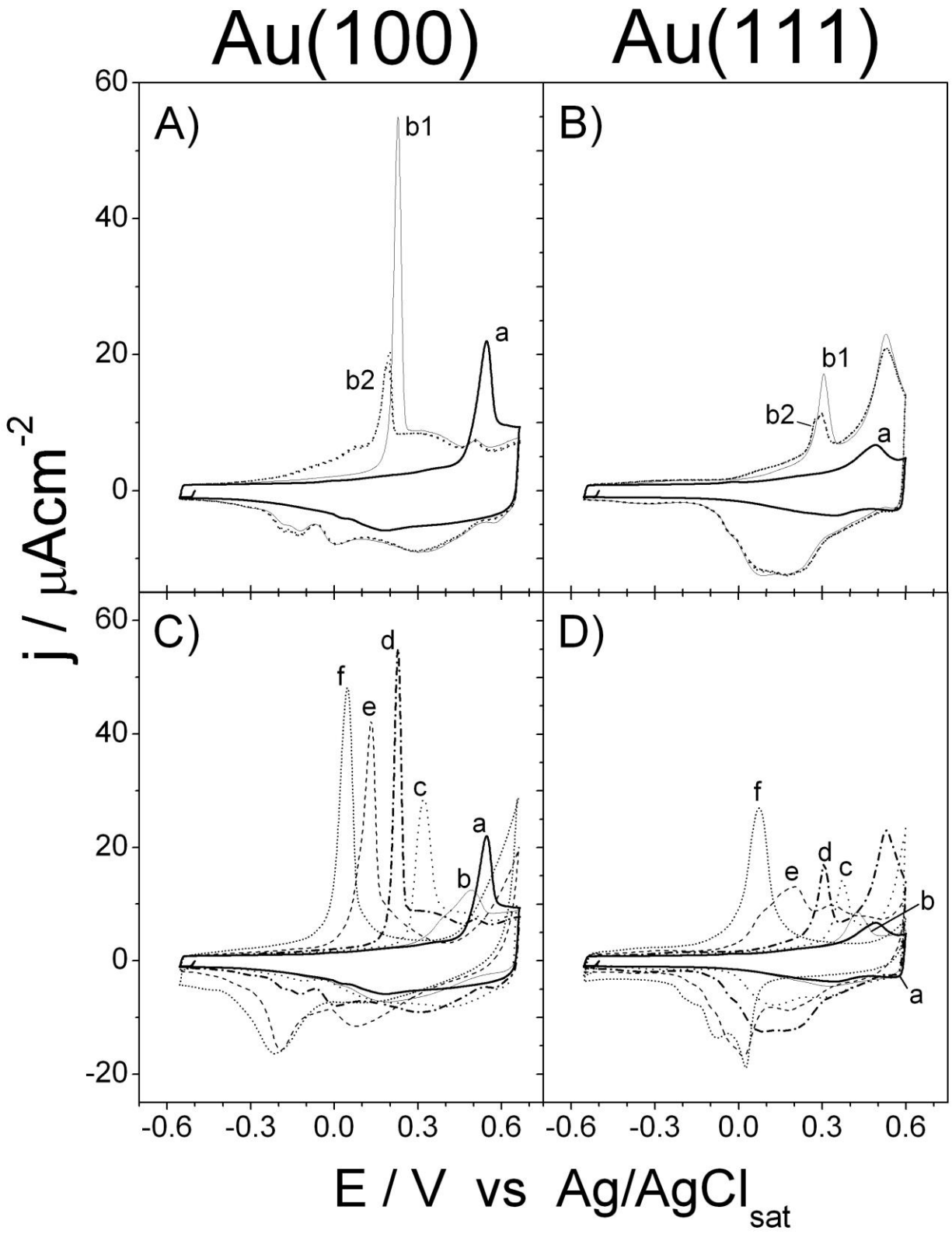
Au(100)
Au(111)
A)
B)
C)
D)
b1
b2
a
b1
b2
a
f
e
d
c
a
b
f
e
d
c
b
a
60
40
20
0
-20
-0.6
-0.3
0.0
0.3
0.6
j / μAcm-2
E / V vs Ag/AgClsat

Figure 1

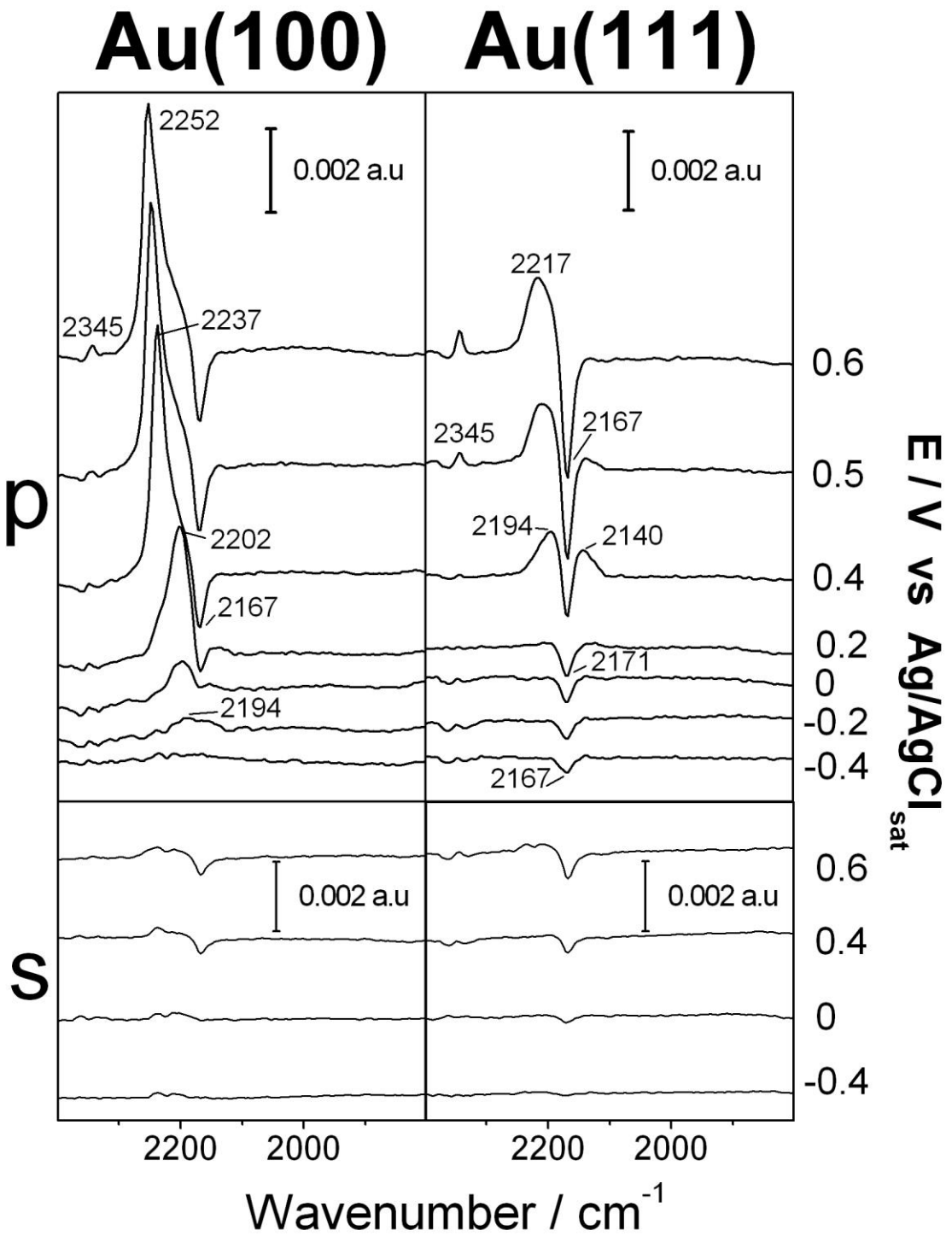
Au(100)
Au(111)
p
s
2252
2345
2237
2202
2167
2194
2217
2167
2140
2171
0.002 a.u
0.6
0.5
0.4
0.2
0
-0.2
-0.4
2200
2000
Wavenumber / cm-1
E / V vs Ag/AgCl sat

Figure 2

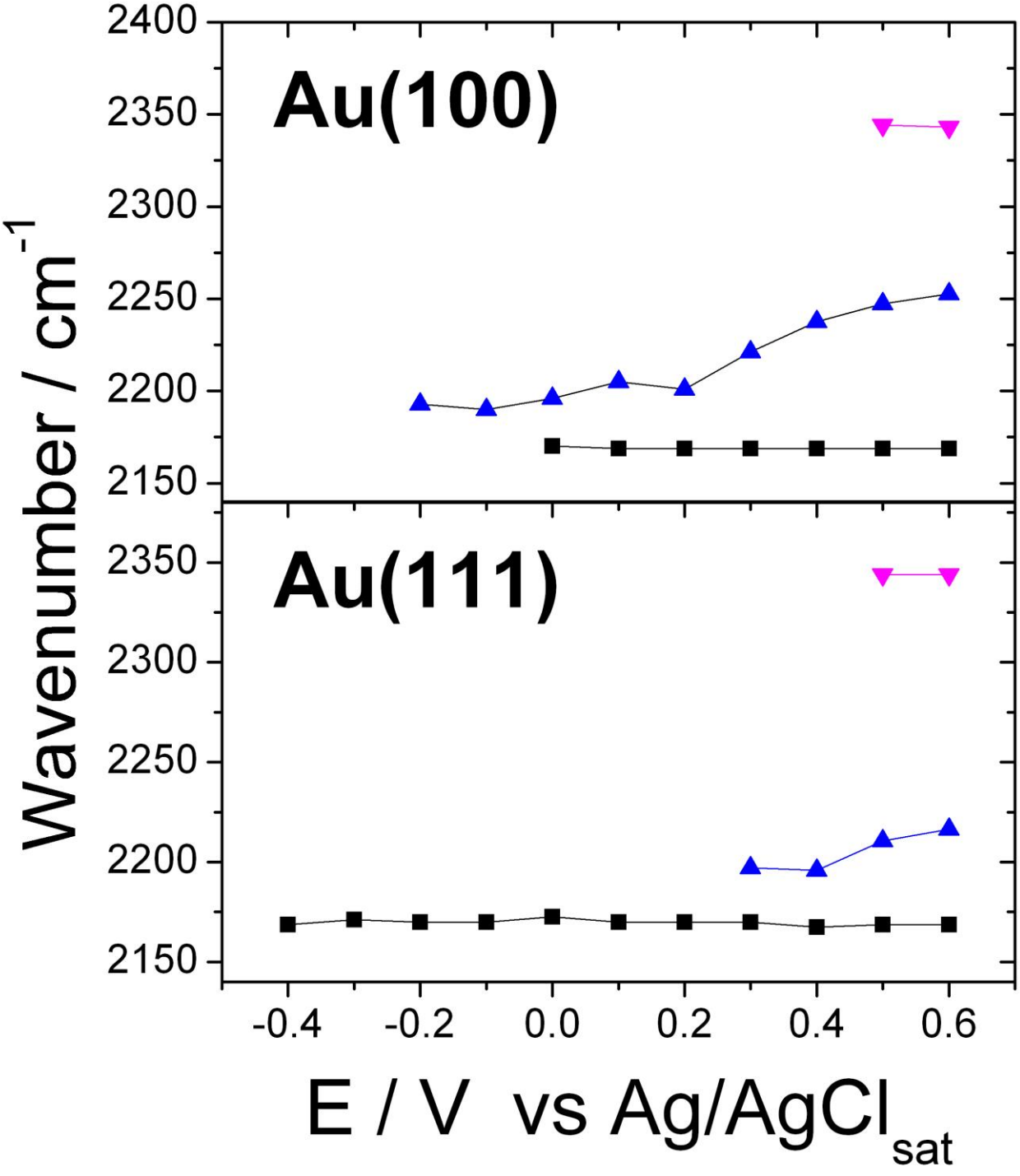

Figure 3

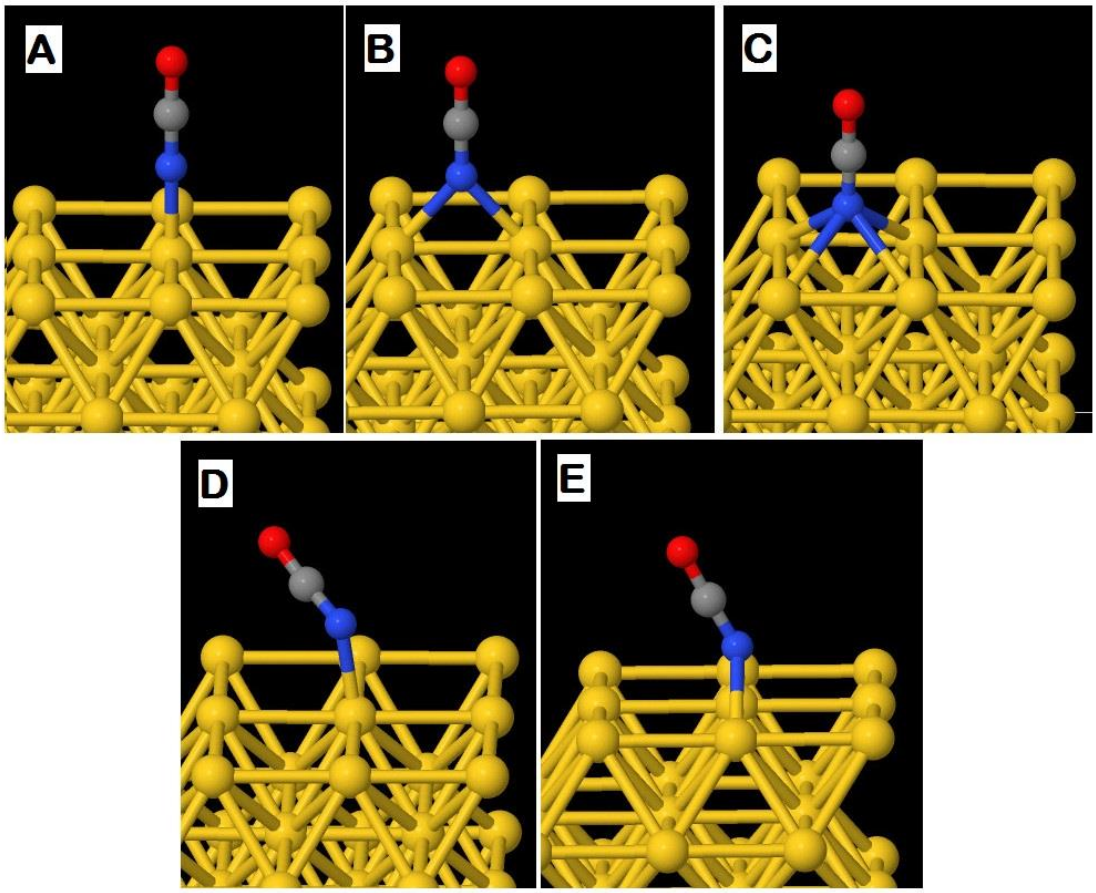

Figure 4

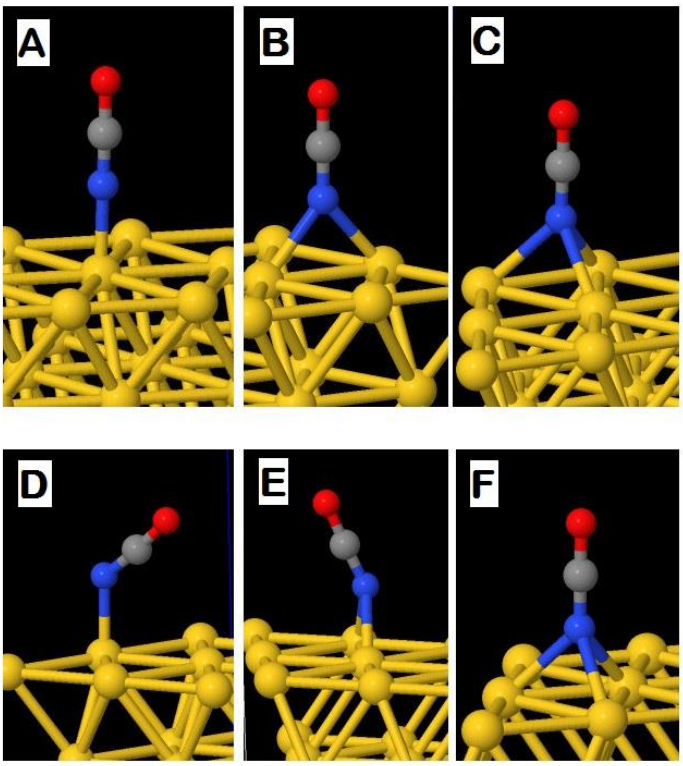

Figure 5

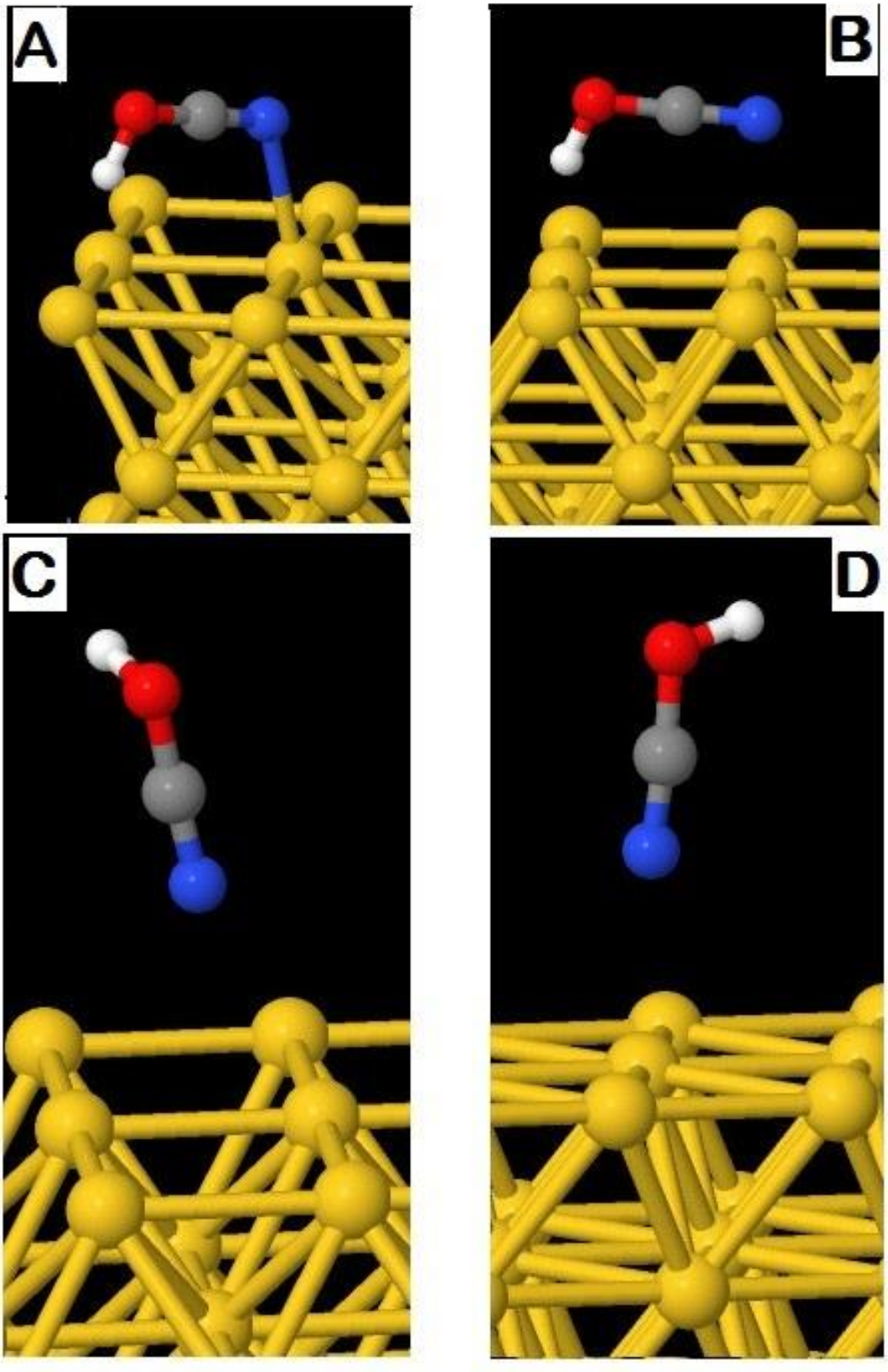

Figure 6

TABLES

Table 1. Optimized geometry and vibrational frequencies of cyanate radical, cyanic acid and isocyanic acid in the gas phase.

	OCN	**HOCN**	**HNCO**
d(NC) / pm	123	117	122
d(CO) / pm	120	131	118
d(HX) / pm	-	98	101
Θ(NCO) / º	180	176	172
Θ (HXC) / º	-	111	125
ν_{asym} (NCO) / cm^{-1}	1983	2301	2310
ν_{sym} (NCO) / cm^{-1}	1253	1297	1194
ν (HX) / cm^{-1}	-	3610	3661

X=N,O

Table 2. Calculated adsorption energies, vibrational frequencies and optimized geometry of N-down, O-down and flat OCN adsorbed on Au(100).

	N-DOWN			O-DOWN			TILTED N-DOWN	
	TOP	BRIDGE	HOLLOW	TOP	BRIDGE	HOLLOW	TILTED TOP	TILTED-BRIDGE
E_{ads} / kJ·mol^{-1}	-186	-216	-193	-73	-94	-96	-193	-216
ν_{asym} (OCN) / cm^{-1}	2267	2231	2171	2094	2184	2140	2162	2200
ν_{sym} (OCN) / cm^{-1}	1352	1315	1272	1205	1160	1124	1295	1296
d(X-Au) / pm	207	221	257	227	240	273	212	224
d(CN) / pm	120	122	123	120	119	119	120	119
d(CO) / pm	120	119	119	124	126	127	122	122
Tilt / º vs normal	0	0	0	0	0	0	61	~ 45

X= N, O

Table 3. Calculated adsorption energies, vibrational frequencies and optimized geometry of N-down, O-down and flat OCN adsorbed on Au(111).

	N-DOWN				O-DOWN				TILTED N-DOWN	
	TOP	BRIDGE	OCTA	TETRA	TOP	BRIDGE	OCTA	TETRA	TILTED TOP	TILTED BRIDGE
E_{ads} / kJ·mol^{-1}	-175	-174	-174	-161	-53	-68	-70	-69	-169	-174
ν_{asym} (OCN) / cm^{-1}	2268	2220	2207	2209	2074	2139	2126	2129	2170	2203
ν_{sym} (OCN) / cm^{-1}	1352	1310	1296	1298	1206	1156	1143	1145	1298	1299
d(X-Au) / pm	208	229	239	240	237	251	263	263	212	230
d(CN) / pm	120	122	122	122	120	119	119	119	122	122
d(CO) / pm	120	119	119	119	124	125	125	125	120	119
Tilt / º vs normal	0	0	0	0	0	0	0	0	50	24

X= N, O

Table 4. Calculated adsorption energies, vibrational frequencies and optimized geometry of cyanic acid (HOCN) adsorbed on Au(111) and Au(100).

	Au(100)			Au(111)			
	TOP	BRIDGE	DOUBLE BRIDGE	TOP	BRIDGE	OCTA	TETRA
E_{ads} / kJ·mol^{-1}	-40	-10	-31	-6,5	-3,9	-3,7	-3,8
ν_{asym} (OCN) / cm^{-1}	2229	2287	2255	2324	2310	2311	2290
ν_{sym} (OCN) / cm^{-1}	1193	1191	1204	1190	1194	1194	1193
d(N-Au) / pm	249	337	314	271	361	370	390
d(CN) / pm	118	117	118	117	117	117	117
d(CO) / pm	128	130	129	130	130	130	130
d(HO) / pm	103	98	101	98	98	98	98
Θ (OCN) / º	179	175	179	176	175	176	175
Θ (HOC) / º	109	111	109	111	111	111	111
Tilt CN axis / º vs normal	76	15	87	6	5	11	13

The molecular dihedral angle in all cases was 180º.